Wanted: A positive control for anomalous subdiffusion

Supporting material 1
Candidate experimental standards: Anomalous subdiffusion

Michael J. Saxton

Department of Biochemistry and Molecular Medicine
University of California
One Shields Ave.
Davis, California

S1.1 Nanofabrication

Nanofabrication is important in applications including electronics, optics, and biophysics. Two general approaches are used. In top-down methods such as photolithography and e-beam lithography, material is removed from a macroscopic substrate. Bottom-up methods use self-assembly. A problem with bottom-up methods is that in many cases self-assembly nucleates at many different points to produce a locally-ordered system with grain structure and dislocations. Longer-range order can be obtained by hybrid methods, in which large-scale structures are made by a top-down approach, and these structures interact with bottom-up components to determine the position and phase of the smaller-scale structures. This templating process also avoids the fundamental theoretical limitation on 2D crystalline order (45). The hybrid method is discussed in more detail in section S1.1.2.2 for block copolymers.

Here we consider methods to make nanopores, nanodots, and nanopillars alike. If a process can make one of these forms, it is likely to be adaptable to make the others (46–48). For example, a hexagonal array of nanospheres can be used as an array of lenses to focus light on photoresist, or as a mask either to give deposits of metal in the interstices or to allow reactive ion etching there. What matters is the geometry of the pattern and the length scales.

For the most part we consider 2D diffusion, but 2D diffusion can be implemented either as a 2D system or as a projection of a 3D system. The most biophysical 2D calibration system is an obstructed phospholipid bilayer. Here the nanofabricated structures can either be the obstacles or binding sites for the actual obstacles, say transmembrane proteins in the bilayer. A useful projected 3D system is diffusion in an aqueous medium obstructed by a "forest" of nanopillars (section S1.1.3.4).

Obstructed diffusion is not controlled by the area fraction of obstacles alone, but by the excluded area fraction, so obstruction can be tuned by varying the size of the diffusing species. Near the percolation threshold, diffusion is far more sensitive to the size dependence of obstruction (49) than to the usual size dependence predicted by the Saffman-Delbrück equation in 2D or the Stokes-Einstein equation in 3D.

The roughness of nanostructures is often measured as the line edge roughness, with 3-standard-deviation values in the 3–10 nm range (50) but fortunately smoothness is less important here because the obstacle roughness is convolved with the tracer shape to give the excluded area.

What obstructed structures are practical to fabricate? We consider four types, in order of decreasing regularity.

S1.1.1 Regular lattice

S1.1.1.1 Nanospheres

A standard approach to making nanostructures is masking with nanoparticles ("colloidal lithography" or "nanosphere lithography"). Uniform nanospheres are deposited on a substrate and form a triangular (hexagonal close-packed) lattice, due to capillary forces during drying and electrostatic forces if the spheres are charged. This preparation is shadowed with, say, gold, producing interstitial deposits, and the nanoparticles are removed to leave a triangular lattice of deposits (51, 52). Alternatively the nanoparticles are used as a mask for wet or reactive ion etching (52). More complex regular patterns can be generated from stoichiometric binary colloidal monolayers prepared using a Langmuir trough (53). Regular lattices of obstacles can also be constructed using block copolymers (section S1.1.2.2) or nanopillars (section S1.1.3.4).

Regular lattices are expected to give transitional transient anomalous subdiffusion over a limited and fixed length scale, so their usefulness is limited. Indeed, Takimoto et al. (54) have made such a pattern using polystyrene beads of diameter 1 or 3 μm as masks, yielding a hexagonal pattern of silver triangles. The pattern was designed as a static model of Kusumi-style corrals (25), in which escape from a corral was by the narrow gaps between the obstacles ("nanogates"). SPT measurements were carried out by total internal reflectance microscopy using a fluorescent lipid analog. The authors observed transient anomalous subdiffusion over ~ 1 order of magnitude in time, that is, transitional anomalous subdiffusion, exactly as argued by Destainville et al. (23) for actual Kusumi-style corrals. The video-rate time resolution did not permit observation of an initial period of normal diffusion. To extend the anomalous range, two approaches are possible: perturbing the lattice (section S1.1.2) and random removal of obstacles (section S1.1.3.5).

S1.1.1.2 Electrochemically etched pores

Electrochemically etched porous materials are often prepared so as to give regular arrays, but they may be useful as templates or for FRAP measurements of single-file diffusion (section S1.3).

One process uses aluminum or titanium as the substrate and yields regular arrays of pores in the metal oxide (55). Some work has sought to maximize length, giving in one case titania nanotubes 1000 μm long (56). Work on nanowire arrays has optimized the porous templates for high density. For example, Zeng et al. (57) made arrays of Co nanowires by electrodeposition in anodized aluminum, with pore diameter 10 nm, center-to-center distance 35 nm, and a density $> 1 \times 10^{11}/\mathrm{cm}^2$, approaching the densities required here.

Another process uses electrochemical etching of doped silicon crystals (or III-V semiconductors) with HF solutions. Number densities of pores ($> 1-2\times10^{12}/\mathrm{cm}^2$) can reach the levels required here. Under appropriate conditions the pores self-organize into a 2D lattice. Pore morphology can range from a regular array of smooth pores to pores with oscillating diameters to fractal pores. For examples of branching and geometric irregularities, see the scanning electron micrographs of Lehmann et al. (58). The pore formation process is complex but well-studied on account of applications in electronics, optoelectronics, optics, and sensors. One of the mechanisms of pore formation is avalanche breakdown. The geometry of the pores (mean diameter and spacing) and the morphology are controlled by several variables. One set of variables specifies the semiconductor properties of the substrate, such as the dopant and the doping level, illumination to generate charge carriers, and the solubility of atoms comprising specific crystallographic planes. Another set of variables specify the electrochemical treatment, such as the electrolyte used and the choice of constant current or constant voltage conditions. For a convenient summary see the introduction to Ouyang et al. (59) and for a comprehensive review including images of a wide variety of pore morphologies see Föll et al. (60).

S1.1.2 Perturbed lattice

Perturbing the lattice could be used to extend the range of transient anomalous subdiffusion but this work must be supported by modeling to give the anomalous diffusion exponent and the crossover time as a function of disorder.

S1.1.2.1 Perturbed nanospheres

The regular lattice formed by adsorbed nanospheres can be perturbed. Binary mixtures of nanospheres have been shown to give quasicrystalline superlattices (61); quasicrystalline structures can also be made by interference lithography (62). The lattice might be perturbed even more by using polydisperse nanospheres. Alternatively one might make a regular lattice of a mixture of soluble and insoluble nanospheres of the same size and strongly adsorbed by the substrate, dissolve the soluble nanospheres, and use the resulting structure as a mask.

S1.1.2.2 Block copolymers

A potentially important method of producing a perturbed lattice is the use of block copolymers (63–66). Block copolymers are a type of amphiphile consisting of two or more different immiscible polymer chains covalently linked at the end, $\mathrm{A}_m\mathrm{B}_n$ for the commonly used diblock copolymer. The covalent linkage forces the separation of the immiscible polymers to be on the length scale of the polymer chains (65).

Some block copolymers can form self-assembled nanostructures in which one of the blocks forms small domains surrounded by regions of the other block, that is, "cores" surrounded by "coronas." These nanostructures are of interest because the length scales are smaller than currently attainable from photolithography, and because self-assembly occurs in parallel. Nanofabrication using e-beam lithography has very high resolution but has to be carried out serially, point by point.

One example of block copolymer self-assembly to give metal nanodots is as follows (67). Dissolve the block copolymer in a solvent that favors one of the blocks, here polystyrene-block-poly(2-vinylpyridine) (PS-b-P2VP) in toluene. Micelles of the P2VP block are formed. Add a metal salt that partitions into the micelles, here HAuCl_4. Deposit the mixture on the substrate, and anneal by thermal or solvent treatment (time scale of days). At this point there is an ordered pattern of micelles containing the metal salt. Use reactive ion etching to remove the copolymer and decompose the metal salt, leaving the corresponding pattern of metal dots.

A variety of other reactions can be used to make this sort of pattern, such as polystyrene-block-poly(methylmethacrylate) (PS-b-PMMA) copolymer with ultraviolet degradation of PMMA to products soluble in acetic acid (68), or polystyrene-polybutadiene copolymers, for which osmium tetroxide labeling can be used to visualise the structures and ozone can be used to remove the diene component (47).

The structure of the phase-separated copolymer can be controlled in various ways:

- The choice of copolymer composition and size. The key parameter is product of the number of monomers in the copolymer and the Flory-Huggins interaction parameter between the blocks.
- Substrate properties. For example, if the substrate is coated with a random polymer of the same average composition as the block copolymer, the surface becomes chemically neutral for the block copolymer.
- The ratio of film thickness to block copolymer length.
- The thermal or solvent annealing procedure, which has been shown to have a major effect on uniformity of size and the regularity of the lattice (69).
- Kinetic trapping.
- Addition of one or both homopolymers (70).

The main goal for applications is semiconductor fabrication so attention has been focused on making a lattice of uniform metal dots homogeneous over the length scale of a

silicon wafer. But here we want nonuniformity. We need to pessimize what most workers in the field seek to optimize!

Typical block copolymer nanostructures in the literature seem to be either a slightly perturbed triangular lattice, or a locally regular triangular lattice with dislocations and grain boundaries. One way to make a more irregular arrangement is the addition of homopolymer to the block copolymer. Stuen et al. (71) carried out a detailed study of the structure of PS-b-PMMA plus both homopolymers, as a function of homopolymer molecular weight and concentration, and the film thickness. They found conditions giving significant variation in domain size, spacing, and regularity, so one could optimize for irregularity. Another potential approach is to use a polydisperse block copolymer. In the PS-b-P2VP case discussed earlier, one could use a polydisperse P2VP core phase to vary the obstacle size and a polydisperse PS corona phase to vary the spacing. The structure might be further tuned by adding polydisperse homopolymers.

Nanostructures uniform over long distances are needed to use the ablation approach (section S1.1.3.5). As mentioned in section S1.1, methods combining top-down and bottom-up approaches have been used extensively in making uniform block copolymer nanostructures (72). This approach is called interpolation (73), density multiplication (74, 75), or templating (64). Cheng et al. (64) nicely summarize the idea in their title "Templated self-assembly of block copolymers. Top-down helps bottom-up." Yang et al. (76) report extensive work on bit-patterned media at a density of 1 Tbit/in^2 made from block copolymers patterned by e-beam lithography. A remarkable scanning electron micrograph of the edge of the patterned region shows a high-quality lattice in the patterned area and a labyrinth structure in the unpatterned area. Block copolymer self-assembly improves the quality of the lithographic patterns, in addition to increasing the attainable densities. These authors describe in detail the effect of various process variables on the quality of the pattern. In all this work, a key parameter is the ratio of the block copolymer length to the template length.

The block copolymer literature includes eye-catching complex structures known as "labyrinths" or "fingerprints" formed by depositing cylindrical micelles flat on the substrate (47, 77, 78). Ideally the structures would just be parallel lines, but in practice there are bends, gaps, and dislocations. Over long length scales, these labyrinths have some of the features that contribute to anomalous subdiffusion in percolation clusters, such as backbends and dead ends. But they do not have the short-range fractal structure of a percolation cluster. Instead in most cases diffusion is close to one-dimensional over short lengths. It might be possible to make labyrinths with a useful degree of short-range disorder using a templated block copolymer with the length scales of the block copolymer and the template sufficiently mismatched (64).

The Groves lab recently demonstrated a block copolymer system directly relevant to the calibration problem (79). They used PS-b-P2VP to fabricate a supported bilayer with an irregular triangular lattice of gold nanoparticles of diameter 5–7 nm and spacing 50–150 nm on a silica or glass substrate.

Two groups have reported SPT of tracers in block copolymers, one predominantly 1D motion along the axis of curved pores (80) and the other 2D confined motion in an array of pores viewed in cross-section (81). These papers show the feasibility of the approach though as expected, anomalous subdiffusion was not reported.

S1.1.3 Random

S1.1.3.1 Biophysical: lipid bilayer

Considerable work has been done on diffusion in obstructed lipid bilayers. To avoid the complications of cushioned bilayers, we restrict attention to simple supported bilayers. Fluorescent lipid analogs ought to be used as tracers so that the tracers are confined to the distal leaflet. To tune the distance from the percolation threshold, it is necessary to vary the size of the tracer headgroup with the hydrophobic region constant. One possibility is GPI-linked lipids; another is a lipid linkable to different-sized headgroups via avidin-biotin or Ni chelate plus a His tag. Linkages are reviewed briefly in Lohmüller et al. (79).

Several types of obstacles can be used. Gel-phase lipid was used in the pioneering work of Vaz, Almeida, and Thompson using the observed percolation threshold to infer microstructure (82). Later work, in the Longo lab, used atomic force microscopy to show the microstructure of the gel phase (83, 84). A related approach would use a supported bilayer with coexisting liquid-ordered and liquid-disordered domains, and a probe excluded from the minority phase. For background on this see Johnston (85). Another possibility is the use of transmembrane proteins immobilized by adsorption to the substrate of a supported bilayer (86), or to flat nanostructures on the substrate. Finally, artificial nanostructures could be used as the obstacles. Tsai et al. (87) made supported bilayers with arrays of linear chromium or titanium barriers, at a spacing of say 250 nm, and gaps of 30, 40, 50 nm length in the barriers. They found free diffusion parallel to the barriers and hindered diffusion perpendicular to them. Tero et al. (88) made supported bilayers on oxide surfaces with random nanostructures: single-crystal TiO_2 surfaces with single atomic steps and terraces, and Si wafers with thermally oxidized surfaces that were rough with peak-to-valley height around 0.5 nm. Transient anomalous subdiffusion was observed, anomalous up to 2 ms, normal to 2 s. The anomalous subdiffusion was attributed to hop diffusion; obstacles and binding sites were specifically excluded. The authors say that at much

higher time resolution, there would be a plateau in the plot of $D(t)$ versus t at short times due to diffusion within the compartments.

The lipid and transmembrane protein obstacles have the advantage of being native membrane components. For artificial obstacles such as metal layers the structure of the bilayer at the obstacle must be considered. One factor is the wetting of the obstacle by the bilayer. In the work mentioned earlier on static corrals, Takimoto et al. (54) used silver triangles as obstacles, and prepared the supported lipid bilayer by spreading to ensure the lipid would not coat the obstacles. They argued that a bilayer made by vesicle fusion would coat both obstacle and substrate. Another factor is the line tension of the bilayer. In bilayer experiments the spatial resolution in the obstructed bilayer might be set by line tension, not obstacle dimensions. The use of bicelle-forming lipid mixtures to suppress line tension might be interesting (89). Whatever the random obstacles, it is necessary to test a square lattice or long rectangles of various sizes to see the effect of the boundaries on diffusion, due to the boundary layers and binding of the tracer to the obstacles.

Horton et al. (5) used FCS to measure the effect of crowding on lateral diffusion of an artificial peripheral protein consisting of avidin bound irreversibly to a biotinylated lipid. Supported bilayers were made with prescribed concentrations of the lipid anchor. When avidin was added, it bound to the biotin. Diffusion of a small fraction of fluorescent-labeled bound avidin was measured. Anomalous subdiffusion began at an avidin area fraction of 3–5 %, a very low value compared to the usual 2D percolation thresholds. The authors attributed the subdiffusion to spatial heterogeneities, specifically the formation of a low-density gel. Avidin is bivalent; similar experiments using a monovalent avidin analog would be informative. This work is noteworthy but not yet understood well enough to be used as a calibration standard.

Czolkos et al. (90) presented a useful general review of supported bilayers, and the review of Kam (91) pointed out differences in artificial obstacles in supported bilayers: chromium blocks diffusion; titanium allows the bilayer to bridge short distances; and carbon nanotubes give partial barriers depending on diameter but their location is difficult to control.

S1.1.3.2 Randomly adsorbed nanospheres

Another approach uses nanospheres. The nanospheres discussed earlier were so weakly bound to the substrate that they could be assembled into a superlattice by capillary forces. To get random nanospheres, a system with stronger binding forces is used so that the nanospheres stick where they first land. For example, negatively charged nanospheres adhered to a substrate made positively charged by adsorbed polyelectrolyte (92, 93). Reilly et al. (93) interpret their results in terms of a percolation model.

S1.1.3.3 Percolation by sputtering

Construction of random nanostructures by sputtering or co-evaporation has a long history in the physics literature, originally as an experimental demonstration of continuum percolation (94, 95), and recently as an example of local near-field enhancement ("hot spots," "surface plasmon localization") (96–98). The original experiment was to deposit a metal onto a dielectric surface, and measure the conductivity as a function of the area fraction of metal. A percolation transition is clearly observed, though this system is not a pure implementation of percolation of random disks on the continuum as in computer simulations. Complications include nucleation, Ostwald ripening, and tunneling effects on conductivity (99), as well as local near-field enhancement effects on fluorescence measurements.

S1.1.3.4 Nanopillars

A very interesting series of papers examined the construction of "forests" of vertically oriented carbon fibers, and showed that these obstacles give rise to transient anomalous subdiffusion (100–103). Briefly, the obstacles were grown by plasma-enhanced chemical vapor deposition using acetylene as the carbon source on a hot substrate with random nanodots of Ni catalyst. Each nanodot gave rise to a single carbon fiber. These fibers are distinct from carbon nanotubes. Nanotubes are single crystals, leading to their remarkable physical properties. The fibers are nested cones of carbon (the so-called herringbone structure) with an overall taper (104). The fibers can be coated conformally with SiO_2 to vary the excluded volume and tracer binding.

The diffusion experiments used an array of nanopillars plus an aqueous phase, with glycerol added for the smaller tracers to adjust the time scale of diffusion. Diffusion was measured by SPT or FRAP. FRAP curves were analyzed by simulations. Both obstruction and binding may be involved in the anomalous subdiffusion, hydrophobic binding for carbon obstacles and hydrophilic for SiO_2-coated obstacles. No binding was detected for fluorescein with SiO_2-coated obstacles. The simulations and experiments emphasized forests that were narrow in one direction relative to the obstacle diameter (5 μm forest with 1.7 μm obstacles) as required for the authors' application. For calibration purposes the obstacle forest must be large in both the x- and y-directions.

The growth process leads to carbon obstacles tapered in the z-direction. This complication ought to be eliminated, either by choosing growth conditions to minimize taper, or by coating with silica (104). The effects of processing conditions on structure have been studied in detail (105).

Alternatively one might use forests of carbon nanotubes instead of carbon fibers. Current work on nanotube forests (106) gives a spacing < 10 nm, a diameter of 2.5 nm, and a surface coverage up to 0.65, all in a useful range for the calibration problem. Forest heights are in the mm range, far higher than needed here. Recent work examines the z-dependence of the dynamics of nanotube forest growth, comprehensively and quantitatively (107).

In an interesting combination of techniques, block copolymers have been used to grow iron nanocatalyst arrays on which carbon nanotube forests were grown. The size of the catalyst domains affects the number of walls in the nanotubes (69).

S1.1.3.5 Continuum percolation in an obstacle lattice

We propose a new experimental approach to the calibration problem, a novel percolation problem of continuum percolation in an obstacle lattice. Consider a regular array of obstacles and a tracer just large enough that it is trapped when it is in an intact cell of obstacles (Fig. S1a). If a prescribed fraction of obstacles is randomly ablated (Fig. S1b), the range of diffusion increases. Eventually enough obstacles are ablated that the system reaches the percolation threshold (Fig. S1c). This problem has not been treated in the percolation literature but is similar enough to standard bond or site percolation that it can be treated in the same way. For uniform obstacle size, the percolation threshold can be found as in Saxton (49).

The obstacle lattice problem maps approximately onto bond percolation on a lattice. The cell interiors play the role of lattice sites; the obstacles play the role of bonds; and ablation of an obstacle turns a nonconducting bond into a conducting one. The problem thus becomes bond percolation on the lattice dual to the obstacle lattice, as in the case of earlier work on diffusion obstructed by the erythrocyte membrane skeleton (108). The dual of a square lattice is a square lattice, and the dual of a triangular lattice is a honeycomb lattice. As a matter of physical realism, we consider the continuum case rather than the lattice approximation. The problem is distinct from the standard continuum percolation problems, in which the obstacles are overlapping, partially overlapping (the Torquato cherry-pit model), or repulsive. The percolation thresholds are known for these cases (109) and will be somewhat different for the lattice ablation problem.

This experimental approach has several advantages. First, it exploits the work done in nanotechnology to make uniform lattices of nanostructures over large areas. Second, selectively ablating individual preformed obstacles is likely to be much easier than fabricating the same final pattern of obstacles from scratch, because the resolution required is approximately the lattice spacing of the obstacles, rather than some small fraction of the obstacle circumference. Third, the obstacle array is a stable structure that can be characterized by electron microscopy and explicitly modeled if necessary. Fourth, the system is highly tunable. The original obstacle lattice gives pure confined diffusion. As obstacles are ablated, the tracer diffuses on finite clusters. Then the system reaches the percolation threshold, and finally one has obstructed diffusion away from the percolation threshold. By analogy with random walks on an obstructed lattice, one would expect transient anomalous diffusion at obstacle concentrations below the threshold and pure anomalous diffusion at the threshold (110). The system is further tunable via the tracer diameter. At a fixed obstacle diameter and concentration, a small tracer would be below the percolation threshold; a medium tracer, at the threshold; and a large tracer, above the threshold.

This sort of obstacle system is similar to the bit-patterned media being developed for computer memory. Here a regular array of nanopillars is constructed, with the tip of each nanopillar coated with magnetic film. Each tip stores an independently accessible bit. Current experimental systems (111) reach densities of 3.3 Tbit/in^2, well within the required range for the calibration problem.

One way to produce the regular array of obstacles is interference lithography, which can make periodic structures in 1D, 2D, and 3D, including uniform square or triangular lattices. Extreme ultraviolet and immersion optics may be required to make a dense enough array, but these processes are much simpler for this application than for semiconductor fabrication (112). Another approach is to use templated block copolymers as discussed earlier (section S1.1.2.2). A valuable source of information on production of uniform high-density arrays is the literature on arrays of nanowires and magnetic nanoparticles (113). For example, Yun et al. (114) made arrays of iron oxide particles and varied the particle diameter from 6 to 25 nm at a constant center-to-center spacing of 40 nm (density $0.6 \times 10^{11}/\text{cm}^2$) by varying the ratio of the iron salt to the micelle-forming block. Other labs made arrays with similar nanowire diameters and higher densities, $1 - 2 \times 10^{11}/\text{cm}^2$, spacing 23 to 35 nm, using block copolymers (115, 116) or anodization (57).

Focused ion beam milling appears to be the best way to remove obstacles selectively (117, 118). Laser ablation would require subdiffraction methods, such as multiphoton absorption (119). There is some precedent for the proposed experiment. Deletion processes have been used to produce cavities and waveguides in photonic crystals, though naturally this work emphasizes structures of a minimum size around the wavelength of light (120). Focused ion beams were used in some of this work; Moran et al. (121) suggest a resolution limit of 10 nm.

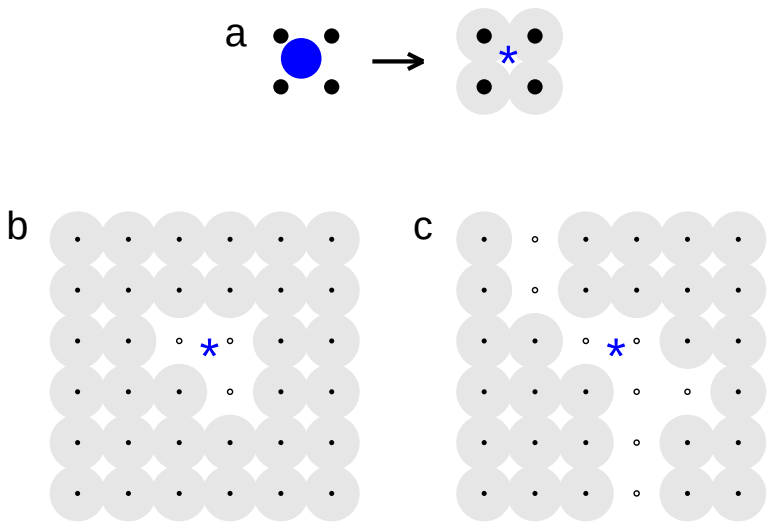

Figure S1: Continuum percolation in an obstacle lattice. Original tracer, *blue circle.* Point tracer, *blue asterisk.* Obstacles, *black circles.* Expanded obstacles, *gray circles.* Ablated obstacles, *open circles. (a),* One cell of obstacles. A tracer of radius R_T and obstacles of radius R_O are equivalent to a point tracer and obstacles of radius $R_T + R_O$. *(b,c),* As obstacles are ablated, the range of diffusion increases and reaches the percolation threshold. This percolation problem is *not* identical to site percolation on a square lattice; ablation of an obstacle may open up a diagonal path as well as x- and y-paths, as shown.

S1.1.3.6 Pinholes

Pinholes in thin films could serve as useful masks. One study found that the distribution of pinhole centers was Poissonian, though the holes and separations were μm-scale, not nm-scale (122). To make nm-scale pinholes, it might be useful to check the literature on how to suppress pinhole defects in resist layers, and do the opposite (123).

S1.1.3.7 Commercial membranes

Commercially available membranes[2] would be highly convenient nanofabrication templates but do not seem to meet the density requirements. Track-etched membranes such as Nucleopore have a nicely random arrangement of pores, and the pores are almost small enough (minimum 15 nm diameter) but the density is too low, in the range 4.5–6.1 $\times 10^8$ pores/cm^2 (124). Custom membranes would be required. Anodization of alumina produces self-organized hexagonal lattices of pores. The spacing in commercial membranes designed as filters (for example Anopore) is too large, but work discussed in section S1.1.1.2 may be applicable.

S1.1.3.8 3D fractal

In very interesting work by Tsujii and collaborators (125, 126), a semi-random 3D silica fractal was constructed with a fractal dimension similar to that of a Menger sponge over the range 0.1–10 μm. First a super-water-repellent structure was made based on the self-assembly of an alkylketene, and then this structure was used as a template for the silica-based structure by a "lost wax" approach.

S1.1.3.9 Random barriers

An alternative model system for anomalous subdiffusion uses a suitable random distribution of barriers. The advantage is that the system does not have to be prepared in a nonequilibrium state. The disadvantage is that diffusion is less anomalous than in the case of binding (127). The problem here is finding a nanoscale physical realization of the mechanism. One possibility is an amorphous solid. Hinze et al. (128) studied states – not diffusion – of a small fluorescent dye in a deeply supercooled polymethylmethacrylate matrix, and discussed their results in terms of a potential energy landscape with basins and metabasins. Problems with such an approach include the time scale of the motion and the complexity of the system. It is a research problem, not a calibration standard.

[2] www.whatman.com

S1.1.4 Arbitrary patterns

Methods that can make arbitrary patterns are appealing. One could use well-understood systems like percolation clusters of penetrable or impenetrable disks on the continuum, or do a physical experiment on a configuration generated from a 2D fluid simulation.

S1.1.4.1 Photolithography

Photolithography is diffraction-limited, with

$$\text{Resolution} = k\lambda/NA, \tag{S5}$$

where λ is the wavelength of light, NA is the numerical aperture of the lens, and k is a constant. Originally $k = 0.61$ from the width of the Airy disk, but now k is taken to be a parameter representing the response of the photoresist under the processing conditions used, and can be decreased by various chemical and optical tricks. Guided by this expression, the semiconductor industry has switched from mercury lines (436 and 365 nm) to excimer lasers (KrF, 248 nm and ArF, 193 nm), used immersion lenses to increase the numerical aperture, and used a variety of other refinements to give a limit around 50 nm. In the photolithography literature, resolution is usually given as the half-pitch, that is, the distance from peak to valley in a line or a fringe (129, 130). In manufacturing, the depth of focus and throughput are important considerations; here they are less so. Extreme UV light has been used experimentally; a 46.9 nm laser in an interference configuration gave lines of 22.5 nm half-pitch (131). Subdiffraction methods using visible light were reviewed by Fourkas (132).

S1.1.4.2 Electron-beam lithography

Electron-beam lithography allows direct writing of arbitrary 2D shapes at high resolution, but it is a serial process that covers small areas slowly. The e-beam can be focused to $<$ 1 nm diameter but the resolution is limited by the interaction of the e-beam with the resist, and the (macro)molecular size of the resist. The review by Grigorescu and Hagen (50) indicates that 10 nm features and spacing can be obtained. This review carefully distinguishes resolution for isolated and dense features. The smallest structures are produced by EBID, electron beam-induced deposition (133, 134).

In biophysical applications, Cherniavskaya et al. (135) made arrays of AuPd dots to study the distance dependence of cell binding to fibronectin. Once the dots were made, the peptides of interest were attached by standard chemistry using thiols and biotin-avidin. The dot size was ~ 5 nm and the spacing 20–100 nm, clearly close to the required range here. An important point emphasized by these authors is how to make double self-assembled monolayers, thiol on the metal dots and silane-poly(ethylene glycol) elsewhere.

Groves, Dustin, and collaborators have done extensive work using μm-scale structures to examine the formation of the immunological synapse and other signaling events (136–138).

S1.2 Binding

Transient binding is a standard model for anomalous subdiffusion. We consider here a finite hierarchy of traps, which gives transient anomalous subdiffusion. Diffusion is anomalous at short times, but normal at long times with $D(\infty)$ determined by the Boltzmann average over Arrhenius escape times from potential energy wells. The crossover time and anomalous subdiffusion exponent depend on the distribution of binding energies in the hierarchy (139). The next sections discuss the two experimental requirements, a hierarchy of binding sites for a fluorescent tracer and a nonequilibrium initial state.

S1.2.1 Arrays of binding sites

The experiment requires a hierarchy of binding sites for the tracer. The general problem of distributions of binding sites is discussed in the literature as adsorption on heterogeneous surfaces, in terms of the affinity spectrum in the biochemical, environmental, and immunological literature, and the adsorption energy distribution in the adsorption literature (140, 141).

The binding sites may be nonbiological or biological. Porous media would be a plausible nonbiological choice. The distribution of binding sites for dyes in various porous media has studied by SPT and FCS (142, 143). In porous glasses, the types of distinct binding sites are limited (144, 145) so the depth of the hierarchy is limited. But what if one deliberately set out to dope a glass or modify the surface to make a wide range of binding sites? For example, a silica or glass surface could be modified using standard silane chemistry. Alternatively ORMOSILs – organically modified silicas – could be used. Here the modification is made to the starting materials, not to the surface after formation (142). Alternatively, inorganic dopants could be used, as studied in connection with mesoporous catalysts (28). Note that SPT and FCS have been used to characterize binding sites in silica that lead to peak broadening and tailing in chromatography (143, 146). Generating a silica-based anomalous diffusion standard is thus another case in which we need to pessimize what the rest of the scientific world tries to optimize. Various treatments are available to identify mechanisms of hindered diffusion in these systems. To isolate the effects of pore geometry, Dozier et al. (147) blocked the binding sites in Vycor by esterification of the silanols with n-propanol. One can suppress van der Waals interactions by refractive index matching, and Coulomb interactions by high ionic strength.

Biological systems – such as arrays of DNA, proteins, or aptamers – have a wide range of binding energies, and the chemistry to make arrays is well-developed (148, 149). Generally these are spatially addressable arrays; the unconventional requirement here is for a mixture random at the level of the individual binding sites. The binding sites must coat the entire surface uniformly, with a prescribed distribution of binding constants and concentrations.

We want to observe motion averaged over many binding sites, not individual binding events. This is readily attained for standard DNA arrays. In a study of DNA surface hybridization regimes, Gong and Levicky (150) used surface densities of 2–16 $\times\, 10^{12}/\mathrm{cm}^2$, chosen as the typical range in applications. Surface densities were measured by hybridization with an electrochemically-tagged oligomer. Similarly, Dandy et al. (151) used a density range 5–12 $\times\, 10^{12}/\mathrm{cm}^2$, measured by ^{32}P radioactivity to give absolute densities. A diffraction-limited spot of 240 nm radius has an area of $1.8 \times 10^{-9}\,\mathrm{cm}^2$, so densities of 2–16 $\times\, 10^{12}/\mathrm{cm}^2$ give 3600–29000 DNA oligomers in the spot.

The required weak and intermediate binding sites are being identified in current work on the energy landscapes of binding. The data needed to design the array must come from an exhaustive method, not from one based on enrichment for strong binding. For an excellent review see Stormo and Zhao (152). Applicable methods include microarrays that cover all DNA sequences of a given size (153), a microfluidic device to measure binding energy landscapes of transcription factors (154, 155), and a commercial sequencer repurposed to give global binding data (156).

A theme in the recent sensor literature is making an array of ligands with different affinities to the target species. The ligands differ in dissociation constant by say an order of magnitude, so that the array binds the target over a much wider concentration range than the individual ligands do (157, 158). A method to isolate aptamers with prescribed binding constants was demonstrated by the Krylov group (159).

Anomalous subdiffusion has been observed in a model system based on DNA-mediated self-assembly (160). A gold surface was coated with DNA having sticky ends, and with a polymer brush to block nonspecific binding. The tracer was a 1.05 μm bead coated with DNA having the complementary sticky ends. Single-particle tracking showed highly anomalous subdiffusion, and the exponent was strongly temperature-dependent. There was no variation in the DNA sticky ends; the observed differences in escape time were attributed to heterogeneities in shape and coverage.

In work on functional immunomics, Braga-Neto and Marques (161) point out that it is difficult to develop a set of antibodies for antibody microarrays, and it would be

much easier to make arrays of antigen peptides and use the antibodies as the mobile species.

Glycan arrays are more complex and less developed than peptide and oligonucleotide arrays (162) but I mention them to suggest the possibility of transient anomalous subdiffusion of glycan-binding proteins due to binding.

S1.2.2 Nonequilibrium state

The other requirement is that the system must be in a nonequilibrium state. In equilibrium, diffusion is normal at all times and slow, at a rate determined primarily by the escape time from the deepest traps. But when the system starts in a nonequilibrium state, there is an initial period of anomalous subdiffusion, corresponding to the search for the deepest traps (139).

How can the initial nonequilibrium state be made? One approach is fast mixing of the tracer with the array of binding sites. This is the approach used by nature in eucaryotic cells when transcription factors are activated, enter the nucleus, and begin to search for their binding sites. Initial mixing with the bulk fluid must be much faster than diffusion in the array.

Another approach is fast photoactivation of the tracer, that is, mixing first and then turning on the interaction with the array. Photoactivatable transcription factors are being developed, for example, (163). This approach requires a large change in binding on photoactivation. Direct photoactivation is better than indirect via an effector molecule, to keep the kinetics of the activation process out of the measurement. Designing a suitable photoactivatable DNA-binding tracer is a nontrivial research problem, but a tractable one given current interest in optogenetics, TAL effectors, zinc finger proteins, and the like (164–167).

S1.2.3 Optical implementations

Optical approaches could be used, such as a laser speckle pattern or an array of laser traps produced by a spatial light modulator (168). It would be highly advantageous to be able to use the modulator to turn the interaction on and off at will, but the key limitation in both approaches is that individual barriers or traps would be on the scale of the wavelength of light, so one would need to use an extremely wide FRAP or FCS beam.

S1.3 Single-file diffusion in pores

A well-known example of anomalous subdiffusion is single-file diffusion, that is, diffusion in a pore so narrow that the tracers cannot pass each other and their order is fixed. This mechanism is important only at high tracer concentrations, a major experimental constraint. Diffusion is anomalous for overdamped systems in the long-time limit because the single-file condition implies that motion of one particle requires collective motion of many other particles in the same direction (169).

The time dependence is as follows. Diffusion is normal at times much shorter than the mean collision time, that is, the diffusion time over the mean separation between tracers. Diffusion becomes anomalous, $\langle r^2 \rangle \propto t^{1/2}$, at longer times. At very long times diffusion again becomes normal if periodic boundary conditions are used in simulations or circular channels are used in experiments (169–171). The pore must be long enough that end effects can be neglected (172). Hydrodynamic interactions among tracers may also affect diffusion (173). The crossover time from normal to anomalous diffusion is tunable via the concentration of tracers but the exponent is constant. One can vary the size of the tracers to go from single-file diffusion to normal diffusion in which tracers can pass.

The pioneering experimental proof of this mechanism was by pulsed field gradient NMR of gases in zeolites (174, 175). An alternative set of experiments is more applicable here. Single-particle tracking was used on μm-sized spheres in channels, either channels made by photolithography (176) or by a scanning optical trap (177, 178). These experiments used μm-diameter spheres so the motion is too slow for the calibration problem. For example, Wei et al. (176) used a paramagnetic polystyrene tracer of diameter 3.6 μm in circular channels of width 7 μm and diameter 33 to 1608 μm. An image was recorded every 8 s for 8 hours, and the crossover times from normal to anomalous diffusion were 10–40 s depending on the interaction, which was adjusted via an external magnetic field. Smaller, faster spheres must be used.

The scaling of diffusion times in the single-file problem is different from the usual diffusion problems so we show an example. Lin et al. (179) presented experimental results and discussed the problem in convenient terms for rescaling. Their experiments were on silica spheres, diameter 1.58 or 3.7 μm, in a groove in a polydimethylsiloxane substrate. The experimental time scale was 30 ms to $\sim$ 900 s, and mean-square displacements were between 10^{-6} and 100 μm^2. How does the time scale shift if we replace the μm-scale sphere with a 40-nm quantum dot?

Following Lin et al. (179), the concentration variables are the 1D number density ρ and the line packing fraction (mean free length)

$$\eta = \rho\sigma, \tag{S6}$$

where σ is the sphere diameter. The mean distance between particles is

$$\ell = (1 - \rho\sigma)/\sigma. \tag{S7}$$

This is the mean closest distance between surfaces; the mean distance between centers is $1/\rho$. The mean collision

time is

$$t_c = \ell^2/2D. \tag{S8}$$

The mean-square displacement is

$$\langle x^2(t)\rangle = 2F\sqrt{t}, \tag{S9}$$

where

$$F = \ell\sqrt{D/\pi} \tag{S10}$$

is the 1D mobility, an anomalous subdiffusion coefficient with units $\mu\mathrm{m}^2/\sqrt{\mathrm{s}}$. The single-file propagator at large times is

$$P_{SF}(x,t) = \frac{1}{\sqrt{4\pi F\sqrt{t}}}\exp[-x^2/4F\sqrt{t}]. \tag{S11}$$

For the rescaling we want a fixed displacement x^2 related to the resolution of an SPT measurement, so we must hold $F\sqrt{t}$ constant. If F is rescaled to aF, then t must be rescaled to t/a^2.

The 1D mobility depends on the diffusion coefficient. For hard spheres, the ordinary infinite-dilution diffusion coefficient is used, but particles with long-range interactions require the collective diffusion coefficient (180). The hard-sphere case is appropriate for uncharged quantum dots with a polyethylene glycol coating to give entropic repulsion. Assume that D follows the Stokes-Einstein law so that

$$D = D_0(\sigma_0/\sigma), \tag{S12}$$

In fact D_0 is less than the Stokes-Einstein value due to friction with the pore walls (173) but for this estimate we assume that D is still $\propto 1/\sigma$. The sphere diameter must be greater than half the pore diameter to maintain the single-file condition, but ought to be only slightly greater in order to reduce hydrodynamic interactions (solvent backflow).

There are two ways to do the rescaling, at constant packing fraction or constant number density. A simple example shows that constant number density is the appropriate choice.

At constant packing fraction, the number density is increased to compensate for the smaller particles, so the free length ℓ decreases considerably. If we reduce the particle size by a factor of α,

$$\sigma_0 \to \sigma_0/\alpha,$$
$$D_0 \to \alpha D_0,$$

then

$$\rho_0 \to \alpha\rho_0,$$
$$\ell_0 \to \ell_0/\alpha,$$
$$F_0 \to F_0/\sqrt{\alpha},$$

so that

$$t_{c0} \to t_{c0}/\alpha^3,$$
$$t \to \alpha t.$$

The large reduction in t_c means that the initial normal diffusion is not detectable, and the increase in t moves the whole measurement in the wrong direction. The increase in number density slows the motion much more than the increase in diffusion coefficient speeds the motion.

At constant ρ, the expressions are more complex because ℓ is changed through σ. The rescaling is straightforward and is best shown by an example. For the data of Lin et al. (179), if we decrease σ from 1.58 μm to 40 nm, D increases from 0.11 to 4.34 $\mu\mathrm{m}^2$/s. For $\eta = 0.57$, we have ρ = 0.361/μm so that ℓ increases from 1.192 μm to 2.730 μm, and F increases by a factor of 14.4. The experimental time scale of 30 ms to 600 s then becomes 150 μs to 3.9 s, and the original collision time of 6.46 s decreases to 0.86 s. So the measurement has been shifted to a more appropriate time scale and the crossover from normal to anomalous is still observable.

What tracers would be appropriate? We need uniform fluorescent spheres. A polymer reptating in a pore is a similar diffusion problem, though a poor choice as a calibration standard because the physics is complicated and specific polymer-pore interactions are likely to be important. One must not use a polymer tracer for which the mechanism of motion depends on concentration.

What experimental conditions are required? In FRAP, the tracers would be microscopic spheres with the fluorophores unstable enough and at a low enough concentration to be photobleachable. One might be able to improve the signal-to-noise ratio by making the measurement on a close-packed array of nanotubes with identical parallel pores. Electrochemically etched arrays can form such an array (section S1.1.1.2), as do some mesoporous materials (section S2.2), such as the M41S and SBA families of molecular sieves, for which the range of pore sizes is 1.6–30 nm (181, 182).

The experimental problem is to ensure that the number of particles in each pore is constant enough not to affect the concentration-dependent mobility significantly. To analyze the experiments, minimally one would need to modify the standard treatment of 1D FRAP for normal diffusion (183) to use the known single-file anomalous diffusion propagator (179). Ideally one would use the full propagator including the normal-to-anomalous crossover (184–186). An FCS or SPT experiment would be done on a single pore. The tracer concentration must be high enough for the single-pore mechanism to work and low enough for FCS or SPT to work, so mixed fluorescent and nonfluorescent spheres must be used. For example, one might use a mixture of quantum dots with a small concentration of fluorescent

dots but with the majority nonfluorescent or with fluorescence distinguishable from the minority. Distinguishable fluorescence would allow measurement of the total tracer concentration so that the mobility can be found. A major constraint on PGSE NMR measurements is having a high enough concentration of the species to be detected (see text, Crosscorrelation).

S1.4 Synthetic motion

By synthetic motion I mean computer-driven physical trajectories in which a stable fluorophore is moved by a piezo stage. Obviously this test is applicable only to SPT and FCS, not to FRAP or PGSE NMR. Synthetic motion has been used in work on single motor proteins (187, 188) and calibration of laser tweezers (189, 190) but ought to be applied to SPT.

Why bother with this? Why not just feed simulated motion plus simulated noise to the SPT or FCS analysis program? Object-plane calibration is useful because it uses the actual response function of the entire optical system, including aberrations, not just an approximation to the point spread function of the objective. One of the standard references on SPT error analysis, Thompson et al. (191), took into account the point spread function of the objective in a Gaussian approximation, shot noise, and pixelation noise at the camera. Everything else was assumed negligible. This approximate treatment is valuable because it captures the main dependencies in simple form. But we need to go farther, if only to show that the approximate treatment works. Another reason for object-plane calibration is that the fluorophore is moved off the optical axis as in an actual trajectory, thus testing the effect of off-axis aberrations. It would be useful to do the full set of tests:

- Artificial motion → signal at camera, to test the model of optics + noise;
- Simulated optical system + simulated noise → trajectory, to test the analysis program;
- Artificial motion → trajectory, to test the entire system end-to-end.

A useful way to improve algorithms for SPT analysis is an open competition among laboratories in which they analyze the same data sets (17, 192) and such a competition is being carried out independently as the Particle Tracking Challenge (193). If only synthetic data sets are used, the winner may well be the algorithm that best simulates the algorithm used to simulate the optics. If real data sets are used, the winner is more likely to be the best algorithm.

The required resolution in space and time is readily attainable. Specifications for one commercial piezo stage[3] (PI P-733.2DD) give a resolution of 0.1 nm and a settling time of 1.36 ms without overshoot for a 30 μm displacement. For similar results in the literature see (187, 188).

The calibration requires a stable immobile point fluorophore. One could use the standard fluorophores from biophysics experiments – fluorescent dyes, intrinsically fluorescent proteins, quantum dots – so that the calibration matches the biological experiment. With no cells to keep alive, the medium can be chosen to minimize photobleaching or blinking (194–196). Another alternative is to use highly photostable species, such as perylene dyes (197) or color centers in diamond (198) among many other possibilities. It might be informative to immobilize the point fluorophore on a nonphotobleachable fluorescent substrate (say uranium glass) to test the response of the system to noise. For measurements at the highest resolution motion of the fluorophore relative to the stage must be eliminated (187) and timing details in the electronics and camera must be considered. Visscher and Block (190) discuss similar timing questions for optical trapping.

S1.5 Polymer solutions

Another potential calibration method is anomalous subdiffusion in polymer solutions (199). We consider a labeled polymer in solvent, a labeled polymer in a polymer solution, and a small tracer in a polymer solution. Polymer labeling may be homogeneous or by a tagged monomer, usually the center, end, or ends. We exclude the case of a tracer in a polymer melt, because diffusion is likely to be slow, the sample must be heated in most cases (except polydimethylsiloxane), and despite the successes of the reptation model, the system is highly complex. Similarly we exclude diffusion in glassy systems. We exclude tracers obstructed by living polymers because this problem requires a time-dependent model of the obstacles in addition to a model of obstructed diffusion. All of these systems are more research problems than calibration standards. Actin gels are discussed on account of their relevance to cell biology.

Polymer systems are appealing for several reasons. First and foremost, they include well-established instances of anomalous subdiffusion. Transverse displacements of semiflexible polymers (200) have $\langle r^2 \rangle \sim t^{3/4}$. The Rouse model describes semidilute systems, where hydrodynamic interactions can be neglected on grounds of screening. For a monomer $\langle r^2 \rangle \sim t^{1/2}$. The Zimm model describes dilute systems, and hydrodynamic interactions are included through a preaveraging approximation. For a monomer $\langle r^2 \rangle \sim t^{2/3}$. Second, one can vary transport properties by varying the solvent among well-defined limits: athermal, good, theta, and bad. Indeed, the Weiss group has interpreted their experimental results for diffusion in cells in terms of solvent quality (201). If nonaqueous solvents are

[3] www.pi-usa.us

to be used, especially in FCS, see (202, 203) and references cited there on the sensitivity of the excitation volume to the solvent through both the refractive index and the aberration corrections of the optics. Third, one can use commercial polymers at least for the preliminary work, though in the highest-accuracy work, custom-made polymers may be needed for uniformity in size and labeling (202). See (204, 205) for further developments of this high-quality work.

The unappealing aspects of polymer systems are the limited range of anomalous subdiffusion and the complexity of the dynamics. A fundamental limitation of using a polymer as the tracer is that diffusion of a labeled monomer may be anomalous at short times, but at long times there is a crossover to normal diffusion of the center of mass of the entire polymer. The crossover time is the Rouse time, which is proportional to the square of the number of monomers, so increasing the polymer size might be useful. The dynamics may be even more complex, with multiple crossovers between diffusive regimes at various characteristic lengths (199, 206). For a spherical tracer in a polymer solution, the exponent varies with time from 1 to 1/2 to 1, and in a reptation model, from 1 to 1/2 to 1/4 to 1/2 to 1. The widths of crossovers must be taken into account. A sensitive test for crossover regions is to find the local exponent $\alpha(t) = d\ln\langle r^2\rangle/d\ln t$ from $\langle r^2(t)\rangle$. For calibration purposes, the anomalous regime ought to have a plateau over a significant time range corresponding to the required length range, with α equal to some known constant. For an example of this analysis see the work of Hinczewski and collaborators (207–209). In many cases their analysis showed exactly the sorts of wide transitions we hope to avoid. To apply this method to FCS results, the correlation curve can be inverted to give $\langle r^2(t)\rangle$, a nicely model-independent approach (5, 210–212). Limits on the spatial resolution must be taken into account (213), but the criticisms of inversion there seem to me less convincing because the examples chosen are of simple transient anomalous subdiffusion, not polymer models with plateaus in α.

A further complication is that in most cases hydrodynamic interactions must be included, and for a polymer tracer in solution, rotational diffusion. McHale and Mabuchi (214), criticized the interpretation of FCS measurements on polymers, arguing that the Rouse and Zimm predictions for FCS curves have so many free parameters that nothing can be proved.

Examination of published experimental results shows that there is clearly a period of anomalous subdiffusion, but only out to $\langle r^2\rangle < 0.5$ μm^2 or less, at least in the publications I have seen. In the work of Bernheim-Groswasser et al. (200) on actin solutions at concentrations near the dilute-semidilute boundary, the crossover to normal diffusion occured around 0.2 μm^2. In the work of Shusterman et al. (210) on single-stranded and double-stranded DNA, the crossover to normal diffusion was ~ 0.1 μm^2. Similar work by Petrov et al. (215) found a different anomalous exponent and argued that much of the apparent power-law behavior is in fact part of the crossover to normal diffusion. The conflict between the two sets of DNA results was addressed using $\alpha(t)$ analysis (207–209), along with theory and simulations that were able to describe the results of Petrov et al. (215) with no free parameters.

Are actin gels suitable, in particular gels with μm-diameter tracers larger than the mesh size, so that the tracers are trapped in actin cages? An advantage is that one can adjust the mesh and tracer sizes; the effects on anomalous subdiffusion were studied systematically by Wong et al. (216). The experiments of Amblard et al. (217) found anomalous subdiffusion from $\langle r^2\rangle = 0.22$ to 2.2 μm^2, in the range we need. Disadvantages are the complexity of the network (218), ambiguity in the interaction between the tracer and the network, and the possibility that the tracer will perturb formation of the surrounding network or crosslink the network locally. Effects of the tracer surface have been studied in detail; see for example He and Tang (219) and references cited there. Despite these potential problems, Amblard et al. (217) found an exponent of 0.73 ± 0.01, close to the theoretical value of 3/4 for semiflexible polymers. I am still hesitant to recommend actin gels; systems that show "a rich mechanical behavior" as a result of dynamics on many length scales (218) do not sound promising as a calibration standard. Actin gels would be better used as the simplest model of cytoplasm (220). For a review of microrheology of cells, including actin gels as models, see Wirtz (221).

Despite all these caveats, interesting results can be obtained using polymer solutions. Omari et al. (222) made FCS measurements of diffusion of 2.5 nm gold nanoparticles in solutions of polystyrene in toluene, using multiphoton excitation of luminescence. The anomalous diffusion exponent decreased from 1.0 to 0.72 as the polymer concentration increased. Subdiffusion began when entanglement did. Diffusion of a small dye, coumarin 480, was normal at all polymer concentrations. Followup work will be of considerable interest.

Wanted: A positive control for anomalous subdiffusion

Supporting material 2
Candidate experimental standards: Obstructed normal diffusion

Michael J. Saxton

Department of Biochemistry and Molecular Medicine
University of California
One Shields Ave.
Davis, California

Even if diffusion is normal at all times, it would be useful to have a standard for obstructed diffusion. We discuss three types: opals, which are geometrically regular; mesoporous structures based on surfactant templates, which may be regular or irregular; and phase-separated glasses, which are irregular. Diffusion in any of these structures may be affected by both obstruction and binding.

According to the excellent review by Gelb (223) on modeling amorphous porous materials, there are two general approaches. In reconstruction methods, the model structure is based on experimental data. The structure is underdetermined so one makes say a random structure constrained by the data. Mimetic methods simulate the physical and chemical processes that produce the material, for example spinodal decomposition for phase-separated glasses. Among other topics the review discusses simulation of phase-separated glasses, sol-gel materials, and templated materials, as well as methods to bring in atomistic detail.

S2.1 Opals

Nanomaterials based on opals have been studied extensively (224). Natural opals are self-assembled superlattices of natural microspheres of hydrated silica. Artificial opals are similar structures made up of monodisperse synthetic microspheres, either inorganic such as silica or alumina, or organic such as polystyrene or polymethylmethacrylate. Inorganic opals can be stabilized by sintering. Inverse opals are a superlattice of voids in a solid, made by filling the interstices of an opal with monomer, initiating polymerization or gelation, and then removing the original microspheres by dissolution or calcination. For example, one could make a polystyrene microsphere opal, infiltrate with a silica precursor, initiate gelation, and finally remove the polystyrene microspheres by calcination. In all these structures the spheres form a close-packed face-centered cubic lattice.

As the play of colors shows, natural opals are made up of particles with a diameter near the wavelength of visible light. Artificial opals are made on a similar scale to make photonic crystals, in which a periodic dielectric microstructure controls photon propagation. For calibration of diffusion measurements, smaller spheres are preferable. For work on these see (225) on making Bragg diffraction filters for the deep ultraviolet, and (226, 227).

An opal or inverse opal is basically a geometrically regular 3D corral model. In the ideal case, diffusion within a void is fast and normal, diffusion from void to void is slow and normal, and a short period of transitional anomalous diffusion connects these limits. In a real inverse opal, if the tracer size is near the neck size, diffusion is sensitive to variation in the diameter of the necks between voids, as discussed by Raccis et al. (228). These authors also give an informative discussion of Brownian dynamics simulations for these systems. For FCS measurements of diffusion of a small dye in an inverse opal, see (30). Theoretical treatments are given by Sofo and Mahan (229) and by Albrecht et al. (230). Torquato (109) treats mostly the "dilute opal" case, in which the spheres are not touching.

S2.2 Mesoporous materials

Alternatively mesoporous materials could be used (28, 231). These materials are well-studied on account of their usefulness as catalysts (181, 182). The materials are typically made by gelation of a silica precursor in the presence of conventional surfactants or block copolymers. In some methods the surfactant self-assembles and acts as a template for the silica; in others the surfactant and silica co-assemble (232). Surfactants may be chosen to yield parallel pores or 3D porous structures. Pore sizes can be controlled by the choice of the surfactant, cosurfactant, and reaction conditions.

The most promising of these structures is the L_3 sponge phase (233, 234). This is a random, isotropic, homogeneous, nonperiodic, bicontinuous phase, optically transparent in these realizations. The pore size is uniform and determined by the solvent volume fraction, with a range of 1–100 nm. Diffusion in a surfactant sponge phase was measured by fringe pattern photobleaching for an amphiphile in the surfactant layer (235) and for a dye and proteins in the aqueous phase (236). FCS measurements of lysozyme obstructed by various structures of a single nonionic surfactant were reported by Szymánski et al. (37).

Bräuchle and collaborators have carried out a remarkable series of SPT experiments on porous media, reviewed by Michaelis and Bräuchle (237) and Lebold et al. (238). One set of experiments correlated tracer trajectories from SPT with the structure of the medium from electron microscopy, an obvious experiment to want to do but a major advance to do. After these validation experiments, SPT was used alone to characterize submicroscopic heterogeneities that would be averaged out in bulk measurements. This work yielded a very detailed picture of the dynamics of the tracer and the properties of the medium, though even at the resolution of SPT the pores and individual defects were often too small to be seen individually.

In most of these experiments, the tracer – a hydrophobic, highly photostable rylene fluorophore – was incorporated into the initial mixture of silica precursor and surfactant before self-assembly. Evaporation-induced self-assembly was used, in which solvent evaporation drives the system above the critical micelle concentration of the surfactant and triggers self-assembly. The surfactant was not removed by calcination or extraction with solvent. The tracer thus diffused in the hydrophobic tails of the surfac-

tant, but the tracer could also interact with sites in the silica phase. Diffusion was sensitive to added solvent vapor (chloroform versus air, for example). The diffusion coefficient could be changed by a factor of 10 by various chemical modifications of the silica surface.

Generally the substrate consisted of pores that were at least locally parallel. Diffusion was predominantly 1D, along the pores. The experiments were able to detect dead ends, defects connecting adjacent pores, and domain boundaries. Periods of immobility were observed, attributed to adsorption sites or narrow holes between pores (239). The pore sizes were small, say 2–3 nm diam, and the tracers were large, for example terrylene diimide, 1.1 nm diameter and 2.5 nm long. The alignment of the tracer with respect to the pore was measured, binding sites were characterized by the emission spectrum of the tracer, and spectral jumps were found to be correlated with orientational jumps (240).

Other surfactant structures such as wormlike chains (partially random) and the cubic phase (a periodic saddle-shaped surface) have been used as templates (231). The pore size from wormlike chains is small (241), at least in the literature I have seen. The high symmetry of the cubic phase is advantageous for diffusion modeling. The sponge phase can be considered a melted or disordered version of the cubic phase.

S2.3 Phase-separated glasses

A more random model system for obstructed diffusion is phase-separated glass such as Vycor or controlled porosity glass (144). Heat treatment of alkali borosilicate glasses leads to phase separation into two continuous phases, one borate-rich and the other almost pure silica. The borate phase can be removed by leaching to give a porous glass. Properties depend on the composition, the temperature of heat treatment, and the cooling rate. Pore sizes are in the range 1–50 nm, although the smallest pore sizes require specialized preparation with fast cooling rates (31, 242). Phase separation is by spinodal decomposition and the modeling is based on this mechanism. One approach uses Gaussian random fields to generate structures matching the observed spatial correlation function of Vycor. With different inputs this model can also be used to generate the symmetric sponge phase (243). Another approach models the process used to produce the porous glass. A mixture of Lennard-Jones particles is equilibrated and quenched. After phase separation has proceeded to the required extent, the system is frozen and the particles corresponding to the borate phase are removed (244).

The fractal nature of phase-separated glasses has been much discussed. Even et al. (245) used FRET experiments to determine the fractal dimension of Vycor. Later work found that the pores are not fractal but the surface may be fractal over a limited range of lengths (246, 247). The fractal nature of the surface may depend on the hydration state (248).

Diffusion of silica tracers in controlled-pore glasses was studied by the Philipse group (249, 250). In one set of experiments both tracers and pores were coated with octadecyl chains so that the only interactions were hard-sphere and hydrodynamic. Measurements were by dynamic light scattering and fringe photobleaching. In the other experiments, tracers and pores were both negatively charged, and diffusion was measured by fringe photobleaching for various electrolyte concentrations. All these experiments were analyzed as normal diffusion. In an important related experiment, Kluijtmans and Philipse (251) showed by FRAP that hydrodynamic interactions are a major factor affecting the diffusion coefficient of spherical silica tracers in a dense random sphere packing, unless the tracer is much smaller than the obstacle size. Diffusion again was taken to be normal.